Nano Research
2022, 15(10): 9663–9669

ISSN 1998-0124 CN 11-5974/O4
https://doi.org/10.1007/s12274-022-4550-9

Research Article

Single-atom catalysts modified by molecular groups for electrochemical nitrogen reduction

Zengxi Wei[1,§], Yuchang Liu[1,§], Hongjie Liu[1], Shaopeng Wang[2,3,4], Minchen Hou[5], Liwei Wang[2,3,4] (✉), Dong Zhai[6], Shuangliang Zhao[1], Kefu Yu[2,4], and Shaolong Zhang[5] (✉)

[1] *Guangxi Key Laboratory of Petrochemical Resource Processing and Process Intensification Technology and School of Chemistry and Chemical Engineering, Guangxi University, Nanning 530004, China*
[2] *School of Marine Sciences, Coral Reef Research Center of China, Guangxi Laboratory on the Study of Coral Reefs in the South China Sea, Guangxi University, Nanning 530004, China*
[3] *MOE Key Laboratory of New Processing Technology for Non-ferrous Metals and Materials, Guangxi Key Laboratory of Processing for Non-ferrous Metals and Featured Materials, Nanning 530004, China*
[4] *Southern Marine Science and Engineering Guangdong Laboratory (Zhuhai), Zhuhai 519080, China*
[5] *College of Chemistry and Environmental Engineering, Shenzhen University, Shenzhen 518060, China*
[6] *Institute of Molecular Sciences and Engineering, Institute of Frontier and Interdisciplinary Science, Shandong University, Qingdao 266237, China*
[§] *Zengxi Wei and Yuchang Liu contributed equally to this work.*

Received: 1 April 2022 / **Revised:** 4 May 2022 / **Accepted:** 15 May 2022

ABSTRACT

Electrochemical nitrogen reduction reaction (eNRR) is one of the most important chemical reactions for the production of ammonia under ambient environment. However, the lack of in-depth understanding of the structure-activity relationship impedes the development of high-performance catalysts for ammonia production. Herein, the density functional theory (DFT) calculations are performed to reveal the structure–activity relationship for the single-atom catalysts (SACs) supported on g-C_3N_4, which is modified by molecular groups (i.e., H, O, and OH). The computational results demonstrate that the W-based SACs are beneficial to produce ammonia with a low limiting potential (U_L). Particularly, the W-OH@g-C_3N_4 catalyst exhibits an ultralow U_L of −0.22 V for eNRR. And the competitive eNRR selectivity can be identified by the dominant *N_2 adsorption free energy than that of *H. Our findings provide a theoretical basis for the synthesis of efficient catalysts to produce ammonia.

KEYWORDS

ammonia, nitrogen reduction reaction, single-atom catalysts (SACs), molecular groups, density functional theory (DFT) calculations

1 Introduction

Ammonia (NH_3) represents an important chemical product for human life, and it is widely used in fertilizer, dye, explosives and so on [1–3]. Undisputedly, the Haber–Bosch approach has the leading status for industrial synthesis of ammonia under harsh conditions, which operates at high temperature (350–550 °C) and pressure (150–350 atm) [4, 5]. This process consumes 2% of global energy and carries 300 million tons of CO_2 emissions per year. Thus, there is an urgent need to to develop sustainable and eco-friendly synthesis technology under ambient conditions to replace the Haber–Bosch approach. Currently, electrochemical synthesis of ammonia has been considered as a promising alternative to the Haber–Bosch approach [5–11]. Electrochemical nitrogen reduction reaction (eNRR) can be carried out by using the easily accessible raw materials of proton source from low-cost aqueous electrolytes and N_2 gas from the atmosphere. However, the eNRR at present suffers from low activity and selectivity due to the intrinsic inactive N≡N bond, in which the ultra-high bond energy of 941 kJ/mol need to be broken [12–16]. Therefore, it is feasible to design and screen efficient catalysts to boost the ammonia yields and Faraday efficiency.

Transition metal single-atom catalysts (TM-SACs) have attracted great attention due to their maximized atom utilization efficiency and outstanding catalytic performance [17–28]. Lots of experimental and theoretical studies have demonstrated that TM-SACs exhibit ultra-high eNRR performance [29–31]. For example, Chen et al. reported that single Mo atom supported by a defective BN monolayer (Mo-BN) exhibits ultra-high catalytic activity for eNRR through an enzymatic mechanism with an overpotential of 0.19 V [32]. Their theoretical results showed that the selective stabilization of *N_2H species and/or destabilizing *NH_2 species are beneficial to produce NH_3. Qiao et al. found that the nitrogen adatom adsorption energy can be a descriptor for the description of the intrinsic activity trends [33]. And the bonding and/or antibonding orbital population regulates the nitrogen adatom adsorption energy. Yang et al. demonstrated that the TM-SACs of Mo_1/N_3-G and Cr_1/N_3-G exhibit outstanding eNRR performance [34]. Their theoretical results identified that the catalytic activity (overpotential) and selectivity on Mo_1/N_3-G and Cr_1/N_3-G are

Address correspondence to Liwei Wang, wangliwei@gxu.edu.cn; Shaolong Zhang, shaolongzhang@outlook.com

0.34 V (40%) and 0.59 V (100%), respectively. As mentioned above, the eNRR catalytic activity and selectivity on TM-SACs can be tailored by modifying the coordination conditions of TMs.

Recently, the solvent effect has attracted wide attention to tailor the catalytic activity and selectivity of electrocatalytic reactions such as hydrogen evolution reaction (HER), oxygen reduction reaction (ORR), and carbon dioxide reduction reaction (CO_2RR) [35–42]. In quantum chemistry field, the solvation effects are generally addressed with explicit, implicit, and mixed implicit/explicit solvent modeling [43, 44]. And the explicit solvent molecules cause the polarization effect and/or synergistic effect during the electrocatalytic reactions. For example, Flaherty et al. found that water and methanol co-catalyze ORR by promoting proton–electron transfer [45]. Their experimental and theoretical results indicated that the adsorbed O_2 molecules can efficiently obtain protons and electrons from resolved methanol molecules on palladium surfaces to produce hydrogen peroxide. At the same time, water oxidizes hydrogen to release hydroxonium ions and electrons to facilitate ORR. Cheng et al. used quantum mechanics molecular dynamics calculations with explicit solvation modeling to analyze the water/Pt(100) interface [36]. Their results predicted that a negative applied voltage could promote the hydrogen binding. And from pH = 0.2 to pH = 12.8, the hydrogen binding is increased by 0.13 eV. Zhao et al. developed an advanced first-principles model to reveal the solid–water interface reaction [37]. They found that the proton affinity to the former/later O in *–O–OH leads to the selectivity dependence on external potential and pH value. The ORR selectivity on single cobalt atom catalyst can be enhanced by decreasing the potential to improve proton adsorption to the former O. However, the proton prefers the latter O at the carbon catalyst in acid condition, leading to poor H_2O_2 performance. These findings demonstrate that solvent environment is critical to interfacial reactions.

Herein, we first introduce the molecular groups, including H, O, and OH, to simulate the solvent environment for eNRR processes. By means of the density functional theory (DFT) calculations, we systematically studied 80 TMs doped in the substrate of g-C_3N_4, which possesses uniformly distributed holes and provides abundant nitrogen coordination numbers, leading to the advantage for trapping metal atoms in the ligands [46–48], for eNRR, respectively. The calculational results demonstrated that the catalytic activity and selectivity for the production of ammonia can be modified by introducing the molecular groups. Particularly, W@g-C_3N_4 modified by the molecular group of OH (W-OH@g-C_3N_4) exhibits ultralow limiting potential of −0.22 V, suggesting the appropriate reaction environment in alkaline solution for the production of ammonia.

2 Calculation details

All computations for geometric optimization were implemented by means of spin polarized DFT using the Vienna *ab initio* simulation package (VASP) [49]. And the related geometries were built by Device Studio program [50], which provided a number of functions for performing visualization, modeling, and simulation. The Perdew–Burke–Ernzerhof (PBE) functional type generalized gradient approximation (GGA) were treated to describe the exchange–correlation interactions between molecule and surface, and the ionic cores were described using the projected augmented wave (PAW) [51, 52]. The van der Waals (vdW) interactions were computed by applying the empirical correction in Grimme's scheme (DFT+D3) [53]. The cut-off energy was set of 520 eV for the plane-wave basis set, and the convergence criteria for the energy and force were set to 10^{-5} eV and 0.02 eV/Å, respectively. To minimize interlayer interactions, the vacuum space was set of 20 Å in the z-direction. The g-C_3N_4 adopted a 2 × 2 × 1 supercell. For structural optimizations, a Γ centered 2 × 2 × 1 Monkhorst–Pack *k*-point sampling was used in the Brillouin zone. Bader charge population analysis was conducted to illustrate atomic charge transfer quantitively in different systems.

Based on the computational hydrogen electrode (CHE) model, the Gibbs free energy change (Δ*G*) of each elementary step was defined as

$$\Delta G = \Delta E + \Delta ZPE - T\Delta S - eU$$

in which Δ*E* denotes the energy obtained from the DFT calculations, ΔZPE and Δ*S* are the correction of zero-point energy and entropy, respectively (summarized in Table S1 in the Electronic Supplementary Material (ESM)), and *T* represents room temperature (298.15 K). The effect of applied electrode potential is contained by the correction of Δ*U*. *e* and *U* are the number of electrons transferred and the applied electrode potential, respectively. Since limiting potential can correlate well with experimental activities for a variety of reductive and oxidative reactions involving proton transfer, we also calculated the limiting potential for the eNRR according to the following equation: $U_L = -\Delta G_{PDS}$, where ΔG_{PDS} is the free energy change of the potential determine step in the NRR.

3 Results and discussion

We first introduce the common g-C_3N_4 as the providential molecular scaffold to trap single metal atom (Fig. 1(a)). To reveal the synergistic effect between molecular groups and TMs, the regular solvent molecules (i.e., H, O, and OH) are taken into account, as shown in Fig. 1(b). We systematically studied 20 TMs binding in g-C_3N_4 substrate to reveal the relationship between catalyst structures and catalytic activity and selectivity on eNRR (Fig. 1(c)).

Theoretical results reveal that the TMs exhibit different coordination number with g-C_3N_4, suggesting the various electron structure of SACs. It can be seen that the relationship of coordination number between TMs and g-C_3N_4 is connected with periodic table of elements. For example, from II B to VII B, there are mainly six coordination numbers between TMs and g-C_3N_4. But four coordination numbers between TMs and g-C_3N_4 play a leading role in VIII B. Additionally, the coordination number can be regulated by introducing molecular groups (i.e., H, O, and OH), as illustrated in Table S2 in the ESM. For instance, the coordination number between W and g-C_3N_4 is six, but the coordination number is replaced by three after introducing O group. The eNRR activity is related to the coordination number of the catalysts. Generally, there are three pathways for eNRR, including distal, alternating, and enzymatic pathways. The previous theoretical results demonstrated that the distal pathway is the preferred reaction mechanism on the TM@g-C_3N_4 catalyst for eNRR. Thus, we explore the eNRR catalytic activity and selectivity on SACs under the distal pathway.

To first evaluate the intrinsic catalytic activity of these SACs, the limiting potential is taken into account. Figure 2 summarizes the negative values of limiting potential for all the 80 SACs, including pristine TM@g-C_3N_4, TM-H@g-C_3N_4, TM-O@g-C_3N_4, and TM-OH@g-C_3N_4 (detailed data are shown in Table S3 in the ESM). For the pristine TM@g-C_3N_4, the theoretical results demonstrate that the W@g-C_3N_4 model has proved to be the optimal catalyst for eNRR with an ultralow limiting potential of −0.52 V, which is in line with previous results [33, 54]. We find that the limiting potentials of these catalysts are less than −1.00 V, including Ti@g-C_3N_4 (−0.70 V), V@g-C_3N_4 (−0.78 V), Zr@g-C_3N_4 (−0.81 V), Nb@g-C_3N_4 (−0.82 V), Mo@g-C_3N_4 (−0.85 V), Ta@g-C_3N_4 (−0.87

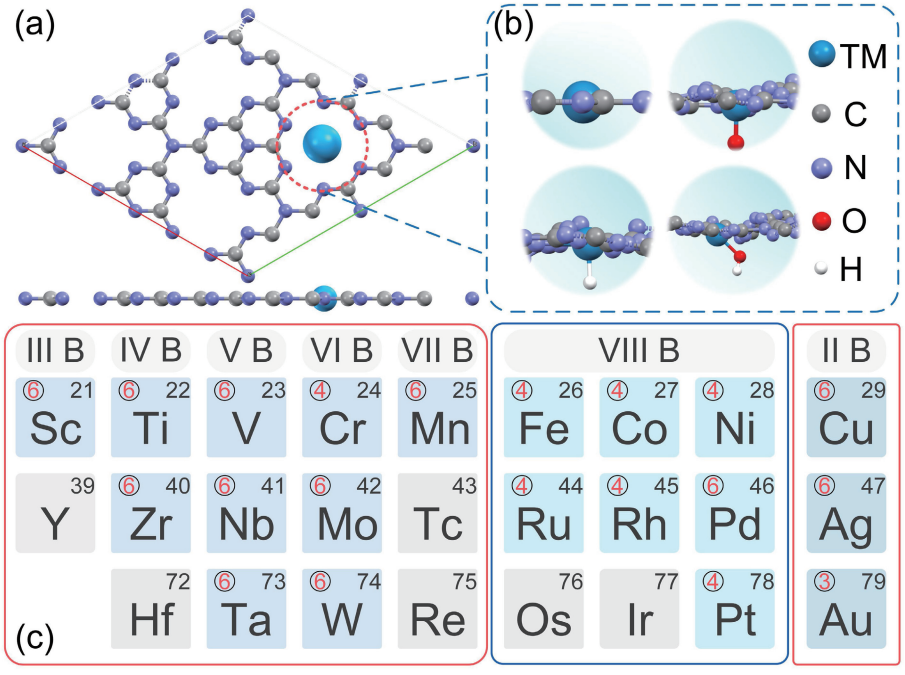

Figure 1 Transition metal single atom catalysts for electrochemical nitrogen reduction reaction. (a) Atomic model of transition metal atom loads on g-C_3N_4 substrate (TM@g-C_3N_4). (b) TM@g-C_3N_4 modified by molecular groups, including of H, O, and OH. (c) Metals, highlighted with a blue background, are considered as the candidates. The numbers in circles represent the coordination number of TMs.

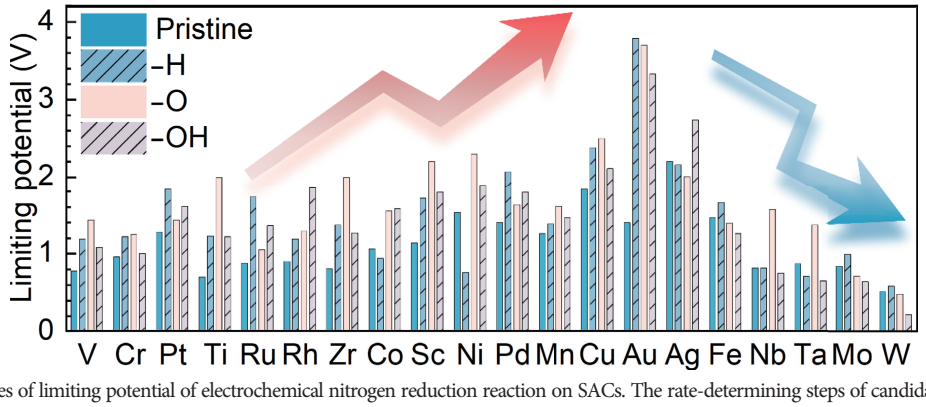

Figure 2 Negative values of limiting potential of electrochemical nitrogen reduction reaction on SACs. The rate-determining steps of candidates are mostly from *N_2 to *N_2H, except for Nb (pristine: *NH_2 to *NH_3), Rh (pristine: *NNH_2 to *NNH_3), Ta (pristine: *NH_2 to *NH_3), and Zr (pristine: *$NHNH_2$ to *NH_2NH_2), respectively.

V), Ru@g-C_3N_4 (–0.90 V), and Cr@g-C_3N_4 (–0.96 V). However, the intrinsic electron structure of TM is changed by the introduced molecular groups of H, O, and OH, leading to the adjustable catalytic activity and selectivity. By introducing the H group, the activity of most catalysts decreases at different levels. For example, the limiting potential on W-H@g-C_3N_4 catalyst increases by –0.07 V than that of W@g-C_3N_4. After binding a H group on the Ru@g-C_3N_4 model, the limiting potential increases by –0.85 V. And an ultrahigh limiting potential can be seen in the Au-H@g-C_3N_4 catalyst (–3.79 V), suggesting the poor catalytic activity for the production of ammonia. On the contrary, by means of H group, the limiting potential of the Co@g-C_3N_4, Ni@g-C_3N_4, Ag@g-C_3N_4 and Ta@g-C_3N_4 decreased by –0.12, –0.77, –0.04 and –0.16 V, respectively.

As can be seen from Fig. 2, the limiting potential can also be decreased by introducing the O group. W-O@g-C_3N_4 catalyst exhibits a lower limiting potential of –0.49 V for eNRR, followed by Mo-O@g-C_3N_4 (–0.72 V), Fe-O@g-C_3N_4 (–1.39 V), and Ag-O@g-C_3N_4 (–2.01 V), respectively. As for the introduction of OH group, the catalytic activities of these catalysts are significantly improved, including W-OH@g-C_3N_4, Ta-OH@g-C_3N_4, Nb-OH@g-C_3N_4, Mo-OH@g-C_3N_4, and Fe-OH@g-C_3N_4. It is worth noting that W-OH@g-C_3N_4 shows the lowest limiting potential of –0.22 V, suggesting the optimal catalyst for the production of ammonia. In addition, both Ta-OH@g-C_3N_4 and Mo-OH@g-C_3N_4 exhibit good catalytic activity with a limiting potential of –0.65 V for eNRR. In general, it is proposed that the W-based SACs can be the potential catalysts for the production of ammonia under various solvent environments (i.e., acidic, alkaline, and neutral solution).

To further understand the reaction mechanism, the free energy diagrams on the W-based SACs, including W@g-C_3N_4, W-H@g-C_3N_4 and W-OH@g-C_3N_4, are plotted in Fig. 3 (other 79 SACs are summarized in the ESM, from Figs. S1 to Fig. S39 in the ESM). Here, the distal mechanism is taken into account for eNRR, in which six proton/electron pairs attack the end and bottom nitrogen atom one by one. It is clear that the intermediates from the distal mechanism are *NNH, *NNH_2, *NNH_3, *N, *NH, and *NH_2, respectively. Fig. 3(a) shows the reaction pathway for eNRR on the W@g-C_3N_4 catalyst. Usually, N_2 adsorption is the first step during eNRR process. The N_2 adsorption process is exothermal with a value of 1.97 eV, suggesting a strong interaction between N_2 and substrate. But the subsequently first hydrogenation process from *NN to *NNH is endothermic with a value of 0.52 eV, which is the rate-determining step (RDS) for eNRR on W@g-C_3N_4. From *NNH_3 to *N, the first ammonia is released with an

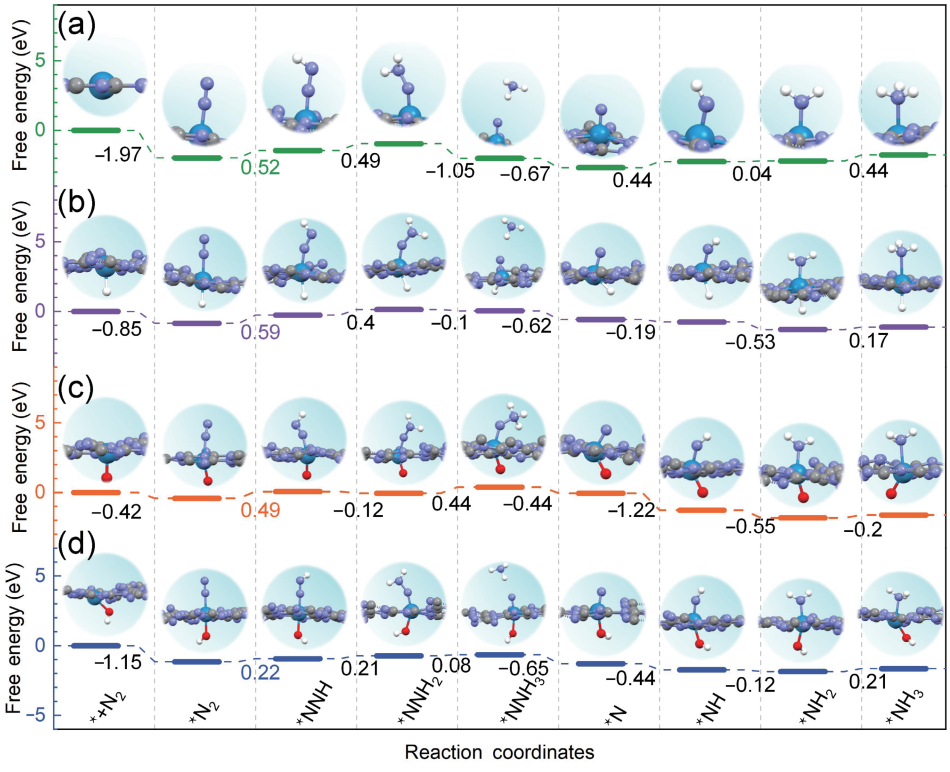

Figure 3 Reaction free energies and optimized geometries on (a) W@g-C_3N_4, (b) W-H@g-C_3N_4, (c) W-O@g-C_3N_4, and (d) W-OH@g-C_3N_4.

exothermal of 0.67 eV. And the release of second ammonia is from *NH_2 to *NH_3, in which the reaction free energy is endothermic of 0.44 eV. By introducing the H group (W-H@g-C_3N_4) (Fig. 3(b)), the N_2 adsorption energy is reduced by 1.12 eV (from W@g-C_3N_4 to W-H@g-C_3N_4). Although the RDS remains the same (from *NN to *NNH), the energy barrier is increased by 0.07 eV. In contrast, the RDS value is decreased by 0.03 eV by introducing the O group (Fig. 3(c)). It is worth noting that the RDS value is only 0.22 eV by introducing the OH group (Fig. 3(d)), which is the optimal catalyst for the production of ammonia. Indeed, these calculation results demonstrate that the alkaline solution is the suitable solvent for eNRR on W-based SACs.

It is worth noting that the relationship between the variational N–N bond length and its Bader charge during the eNRR. Indeed, the stretching of the N–N bond represents the activation process of nitrogen. Fig. 4(a)–4(d) show that as the hydrogenation process occurs, the N–N bond length is obviously stretched (summarized in Tables S4 and S5 in the ESM). Meanwhile, the Bader charge increases dramatically, suggesting the existed reduction reaction process. Moreover, the more Bader charge is obtained, the higher activation degree of nitrogen. For example, the N_2 molecule adsorption on W-OH@g-C_3N_4 can obtain 0.39 $|e|$ with the N–N bond length stretches to 1.15 Å (1.10 Å for relaxing N_2 molecule). After hydrogenation to form *NNH species, the N–N bond length stretches to 1.24 Å, and the intermediate of *NNH obtains 1.13$|e|$, suggesting the ultrahigh N–N bond activation of N_2 molecule, leading to the optimal activity of W-OH@g-C_3N_4 for production of ammonia.

As can be seen in Fig. 5, in addition, the variation of Bader charges from *NN to *NNH (δ_{NN-NNH}) can serve as a descriptor to reveal the catalytic activity for eNRR. The linear relation between δ_{NN-NNH} and limiting potential (U_L) demonstrates that the more variation of Bader charges for intermediates, the smaller U_L for eNRR.

It is well known that HER is one of the critical side reactions, in which the proton/electron pairs are consumed and lead to low

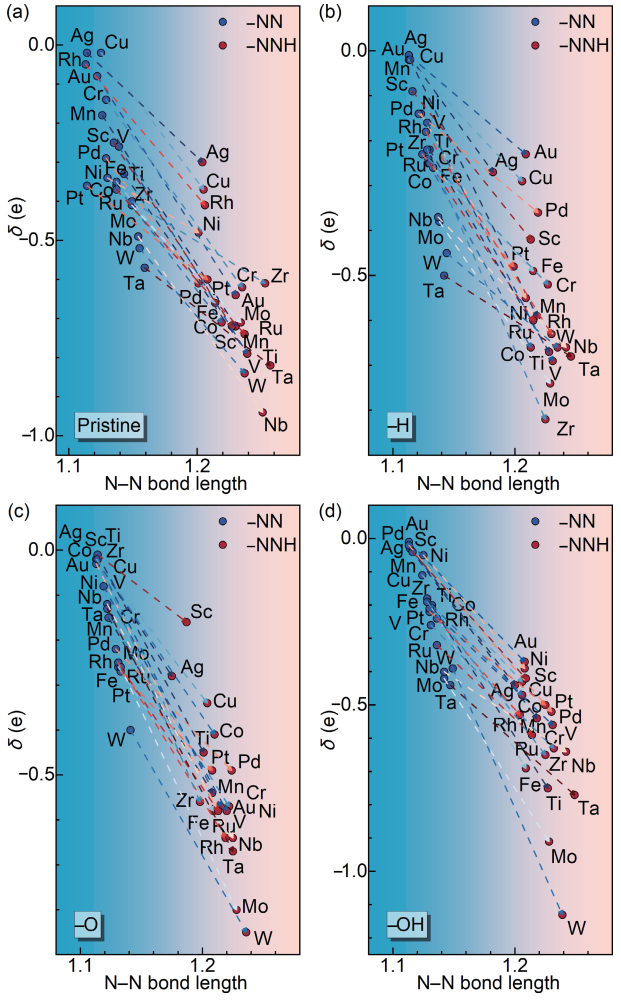

Figure 4 (a)–(d) Computed N–N bond length d_{N-N} and corresponding Bader charge variation (δ) of the intermediates of *NN and *NNH on various TM@g-C_3N_4 SACs, where pristine, *H, *O, and *OH stands for clean, H modified, O modified, and OH modified TM@g-C_3N_4 SACs, respectively.

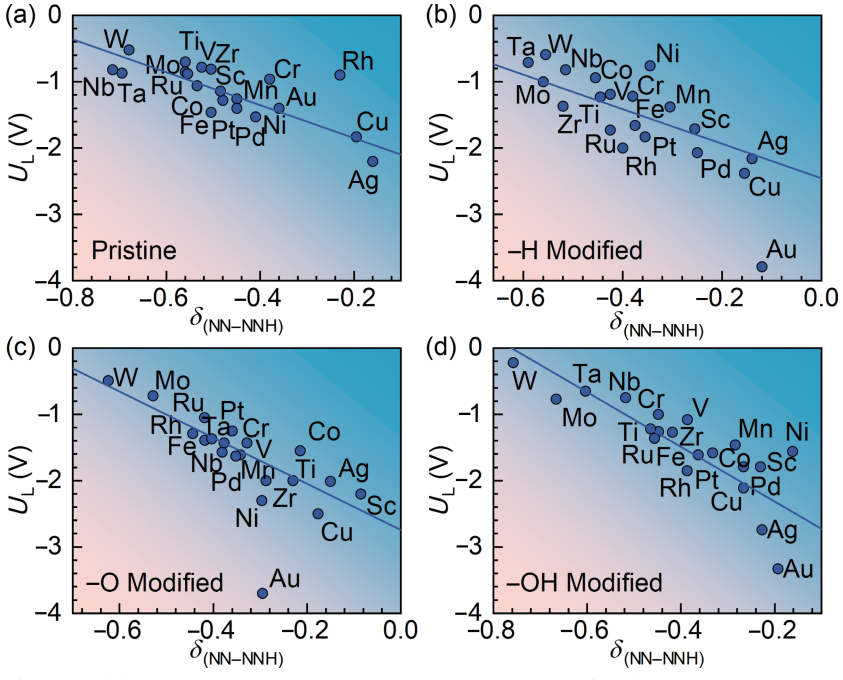

Figure 5 Limiting potentials of SACs, including TM@g-C_3N_4 (pristine) (a), TM-H@g-C_3N_4 (–H modified) (b), TM-O@g-C_3N_4 (–O modified), and TM-H@g-C_3N_4 (–OH modified) (c), plotted as a function of Bader charges variation ($\delta_{NN–NNH}$) (d).

Faraday efficiency (FE). To further reveal the eNRR selectivity, the competitive adsorption free energies for *H and *N_2 are taken into account. As shown in Fig. 6, the catalysts located above the black line represent optimum eNRR selectivity. For the pristine TM@g-C_3N_4 catalysts, only these catalysts exhibit stronger *H adsorption energies than that of *N_2, including Ru@g-C_3N_4, Rh@g-C_3N_4, and Au@g-C_3N_4, leading to low FE. After introducing H group, almost all the catalysts tend to the production of ammonia, except Ni-H@g-C_3N_4, suggesting the acidic solution is more favorable for enhancing FE. But for TM-O@g-C_3N_4, these catalysts, including W-O@g-C_3N_4, Ru-O@g-C_3N_4, Mo-O@g-C_3N_4, Co-O@g-C_3N_4, Rh-O@g-C_3N_4, and Pt-O@g-C_3N_4, are beneficial to release H_2. As for the TM-OH@g-C_3N_4 catalysts, only Pt-OH@g-C_3N_4 is nondominant for eNRR, leading to low FE. It is clear that the W-based SACs, except for the W-O@g-C_3N_4 catalyst, are competitive to release ammonia with higher N_2 adsorption free energy than that of *H, leading to a higher FE. Thus, the W-OH@g-C_3N_4 catalyst can be as a candidate for ammonia production.

4 Conclusions

In summary, we have systematically studied 80 SACs for eNRR, including TM@g-C_3N_4, TM-H@g-C_3N_4, TM-O@g-C_3N_4, and TM-OH@g-C_3N_4. The calculation results reveal that the eNRR activity and selectivity on the TM@g-C_3N_4 catalysts can be modified by introducing molecular groups (i.e., H, O, and OH). Accordingly, these catalysts, including Fe, Nb, Ta, Mo, and W-based catalysts, exhibit favorable catalytic activity for the production of ammonia by introducing molecular groups. And the W-based SACs have

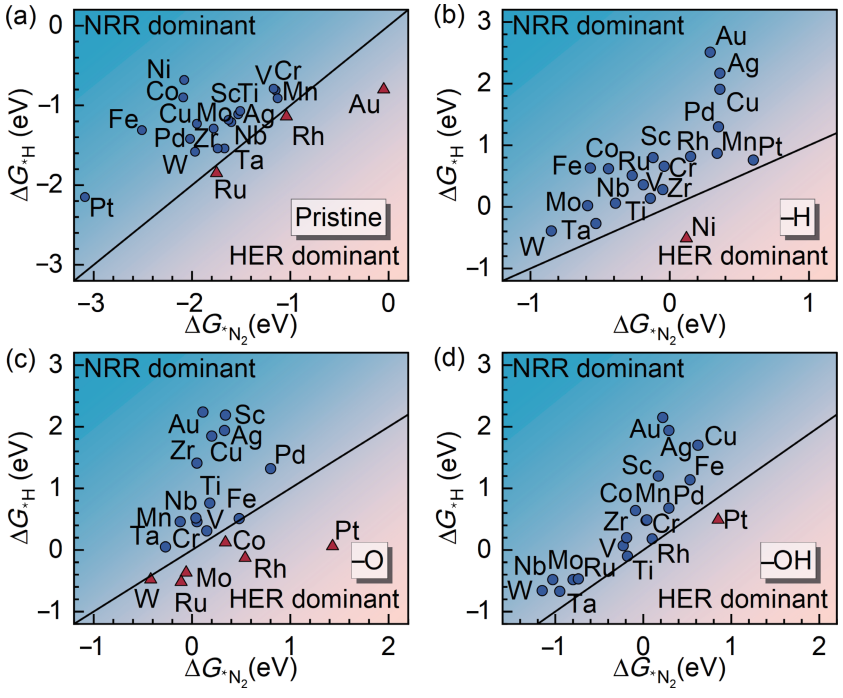

Figure 6 (a)–(d) Calculated adsorption free energies of *H and *N_2 on SACs. SACs above the black line represent the dominant eNRR.

proved to be optimal catalyst for eNRR to produce ammonia. In particular, the W-OH@g-C_3N_4 catalyst shows an ultralow limiting potential of –0.22 V, suggesting its outstanding catalytic activity for the ammonia production. Moreover, the results demonstrate that the N_2 adsorption free energy on W-OH@g-C_3N_4 is higher than that of hydrogen, suggesting the acceptable selectivity for ammonia production.

Acknowledgements

This work was supported by the National Natural Science Foundation of China (Nos. 91934302, 51762005, and 21878078), Key Projects of Guangxi Natural Science Foundation (No. 2020GXNSFDA297015), the China Postdoctoral Science Foundation (No. 2020M683617XB), and the Opening Project of Guangxi Key Laboratory of Petrochemical Resource Processing and Process Intensification Technology (No. 2020K006). Density functional theory calculations were supported by the high-performance computing platform of Hongzhiwei and Guangxi University, Guangxi Postdoctoral Innovative Talents Support Program and Guangxi Science and Technology Base and Talent Special Project.

Electronic Supplementary Material: Supplementary material (geometries and free energy diagrams of single atom catalysts) is available in the online version of this article at https://doi.org/10.1007/s12274-022-4550-9.

References

[1] Burford, R. J.; Fryzuk, M. D. Examining the relationship between coordination mode and reactivity of dinitrogen. *Nat. Rev. Chem.* **2017**, *1*, 0026.

[2] van der Ham, C. J. M.; Koper, M. T. M.; Hetterscheid, D. G. H. Challenges in reduction of dinitrogen by proton and electron transfer. *Chem. Soc. Rev.* **2014**, *43*, 5183–5191.

[3] Rosca, V.; Duca, M.; de Groot, M. T.; Koper, M. T. M. Nitrogen cycle electrocatalysis. *Chem. Rev.* **2009**, *109*, 2209–2244.

[4] Martín, A. J.; Shinagawa, T.; Pérez-Ramírez, J. Electrocatalytic reduction of nitrogen: From Haber–Bosch to ammonia artificial leaf. *Chem* **2019**, *5*, 263–283.

[5] Guo, C. X.; Ran, J. R.; Vasileff, A.; Qiao, S. Z. Rational design of electrocatalysts and photo(electro)catalysts for nitrogen reduction to ammonia (NH_3) under ambient conditions. *Energy Environ. Sci.* **2018**, *11*, 45–56.

[6] Cao, N.; Zheng, G. F. Aqueous electrocatalytic N_2 reduction under ambient conditions. *Nano Res.* **2018**, *11*, 2992–3008.

[7] Fei, H. L.; Dong, J. C.; Chen, D. L.; Hu, T. D.; Duan, X. D.; Shakir, I.; Huang, Y.; Duan, X. F. Single atom electrocatalysts supported on graphene or graphene-like carbons. *Chem. Soc. Rev.* **2019**, *48*, 5207–5241.

[8] Wang, S. Y.; Ichihara, F.; Pang, H.; Chen, H.; Ye, J. H. Nitrogen fixation reaction derived from nanostructured catalytic materials. *Adv. Funct. Mater.* **2018**, *28*, 1803309.

[9] Minteer, S. D.; Christopher, P.; Linic, S. Recent developments in nitrogen reduction catalysts: A virtual issue. *ACS Energy Lett.* **2019**, *4*, 163–166.

[10] Patil, S. B.; Wang, D. Y. Exploration and investigation of periodic elements for electrocatalytic nitrogen reduction. *Small* **2020**, *16*, 2002885.

[11] Zhang, C. H.; Wang, Z.; Lei, J. C.; Ma, L.; Yakobson, B. I.; Tour, J. M. Atomic molybdenum for synthesis of ammonia with 50% Faradic efficiency. *Small* **2022**, *18*, 2106327.

[12] Seh, Z. W.; Kibsgaard, J.; Dickens, C. F.; Chorkendorff, I.; Nørskov, J. K.; Jaramillo, T. F. Combining theory and experiment in electrocatalysis: Insights into materials design. *Science* **2017**, *355*, eaad4998.

[13] Medford, A. J.; Wellendorff, J.; Vojvodic, A.; Studt, F.; Abild-Pedersen, F.; Jacobsen, K. W.; Bligaard, T.; Nørskov, J. K. Assessing the reliability of calculated catalytic ammonia synthesis rates. *Science* **2014**, *345*, 197–200.

[14] Montoya, J. H.; Seitz, L. C.; Chakthranont, P.; Vojvodic, A.; Jaramillo, T. F.; Nørskov, J. K. Materials for solar fuels and chemicals. *Nat. Mater.* **2017**, *16*, 70–81.

[15] McEnaney, J. M.; Singh, A. R.; Schwalbe, J. A.; Kibsgaard, J.; Lin, J. C.; Cargnello, M.; Jaramillo, T. F.; Nørskov, J. K. Ammonia synthesis from N_2 and H_2O using a lithium cycling electrification strategy at atmospheric pressure. *Energy Environ. Sci.* **2017**, *10*, 1621–1630.

[16] Singh, A. R.; Rohr, B. A.; Schwalbe, J. A.; Cargnello, M.; Chan, K.; Jaramillo, T. F.; Chorkendorff, I.; Nørskov, J. K. Electrochemical ammonia synthesis—The selectivity challenge. *ACS Catal.* **2017**, *7*, 706–709.

[17] Nie, L.; Mei, D. H.; Xiong, H. F.; Peng, B.; Ren, Z. B.; Hernandez, X. I. P.; DeLaRiva, A.; Wang, M.; Engelhard, M. H.; Kovarik, L.; Datye, A. K.; Wang, Y. Activation of surface lattice oxygen in single-atom Pt/CeO_2 for low-temperature CO oxidation. *Science* **2017**, *358*, 1419–1423.

[18] Boucher, M. B.; Zugic, B.; Cladaras, G.; Kammert, J.; Marcinkowski, M. D.; Lawton, T. J.; Sykes, E. C. H.; Flytzani-Stephanopoulos, M. Single atom alloy surface analogs in $Pd_{0.18}Cu_{15}$ nanoparticles for selective hydrogenation reactions. *Phys. Chem. Chem. Phys.* **2013**, *15*, 12187–12196.

[19] Qiao, B. T.; Wang, A. Q.; Yang, X. F.; Allard, L. F.; Jiang, Z.; Cui, Y. T.; Liu, J. Y.; Li, J.; Zhang, T. Single-atom catalysis of CO oxidation using Pt_1/FeO_x. *Nat. Chem.* **2011**, *3*, 634–641.

[20] Fei, H. L.; Dong, J. C.; Feng, Y. X.; Allen, C. S.; Wan, C. Z.; Volosskiy, B.; Li, M. F.; Zhao, Z. P.; Wang, Y. L.; Sun, H. T. et al. General synthesis and definitive structural identification of MN_4C_4 single-atom catalysts with tunable electrocatalytic activities. *Nat. Catal.* **2018**, *1*, 63–72.

[21] Lin, L. L.; Zhou, W.; Gao, R.; Yao, S. Y.; Zhang, X.; Xu, W. Q.; Zheng, S. J.; Jiang, Z.; Yu, Q. L.; Li, Y. W. et al. Low-temperature hydrogen production from water and methanol using Pt/α-MoC catalysts. *Nature* **2017**, *544*, 80–83.

[22] Zhang, S. L.; Ao, X.; Huang, J.; Wei, B.; Zhai, Y. L.; Zhai, D.; Deng, W. Q.; Su, C. L.; Wang, D. S.; Li, Y. D. Isolated single-atom Ni-N_5 catalytic site in hollow porous carbon capsules for efficient lithium-sulfur batteries. *Nano Lett.* **2021**, *21*, 9691–9698.

[23] Zhou, G. M.; Zhao, S. Y.; Wang, T. S.; Yang, S. Z.; Johannessen, B.; Chen, H.; Liu, C. W.; Ye, Y. S.; Wu, Y. C.; Peng, Y. C. et al. Theoretical calculation guided design of single-atom catalysts toward fast kinetic and long-life Li-S batteries. *Nano Lett.* **2020**, *20*, 1252–1261.

[24] Wang, Y.; Zheng, X. B.; Wang, D. S. Design concept for electrocatalysts. *Nano Res.* **2022**, *15*, 1730–1752.

[25] Xiong, Y.; Sun, W. M.; Han, Y. H.; Xin, P. Y.; Zheng, X. S.; Yan, W. S.; Dong, J. C.; Zhang, J.; Wang, D. S.; Li, Y. D. Cobalt single atom site catalysts with ultrahigh metal loading for enhanced aerobic oxidation of ethylbenzene. *Nano Res.* **2021**, *14*, 2418–2423.

[26] Yang, J. R.; Li, W. H.; Xu, K. N.; Tan, S. D.; Wang, D. S.; Li, Y. D. Regulating the tip effect on single-atom and cluster catalysts: Forming reversible oxygen species with high efficiency in chlorine evolution reaction. *Angew. Chem.* **2022**, *134*, e202200366.

[27] Zhang, E. H.; Tao, L.; An, J. K.; Zhang, J. W.; Meng, L. Z.; Zheng, X. B.; Wang, Y.; Li, N.; Du, S. X.; Zhang, J. T. Engineering the local atomic environments of indium single-atom catalysts for efficient electrochemical production of hydrogen peroxide. *Angew. Chem., Int. Ed.* **2022**, *61*, e202117347.

[28] Wang, Y.; Zheng, M.; Li, Y. R.; Ye, C. L.; Chen, J.; Ye, J. Y.; Zhang, Q. H.; Li, J.; Zhou, Z. Y.; Fu, X. Z. et al. p–d orbital hybridization induced by a monodispersed Ga site on a Pt_3Mn nanocatalyst boosts ethanol electrooxidation. *Angew. Chem., Int. Ed.* **2022**, *134*, e202115735.

[29] Huang, P. C.; Liu, W.; He, Z. H.; Xiao, C.; Yao, T.; Zou, Y. M.; Wang, C. M.; Qi, Z. M.; Tong, W.; Pan, B. C. et al. Single atom accelerates ammonia photosynthesis. *Sci. China Chem.* **2018**, *61*, 1187–1196.

[30] Légaré, M. A.; Bélanger-Chabot, G.; Dewhurst, R. D.; Welz, E.; Krummenacher, I.; Engels, B.; Braunschweig, H. Nitrogen fixation and reduction at boron. *Science* **2018**, *359*, 896–900.
[31] Jing, H. Y.; Zhu, P.; Zheng, X. B.; Zhang, Z. D.; Wang, D. S.; Li, Y. D. Theory-oriented screening and discovery of advanced energy transformation materials in electrocatalysis. *Adv. Powder Mater.* **2022**, *1*, 100013.
[32] Zhao, J. X.; Chen, Z. F. Single Mo atom supported on defective boron nitride monolayer as an efficient electrocatalyst for nitrogen fixation: A computational study. *J. Am. Chem. Soc.* **2017**, *139*, 12480–12487.
[33] Liu, X.; Jiao, Y.; Zheng, Y.; Jaroniec, M.; Qiao, S. Z. Building up a picture of the electrocatalytic nitrogen reduction activity of transition metal single-atom catalysts. *J. Am. Chem. Soc.* **2019**, *141*, 9664–9672.
[34] Zhao, W. H.; Zhang, L. F.; Luo, Q. Q.; Hu, Z. P.; Zhang, W. H.; Smith, S.; Yang, J. L. Single $Mo_1(Cr_1)$ atom on nitrogen-doped graphene enables highly selective electroreduction of nitrogen into ammonia. *ACS Catal.* **2019**, *9*, 3419–3425.
[35] Cao, Y. Y.; Zhao, J. Y.; Zhong, X.; Zhuang, G. L.; Deng, S. W.; Wei, Z. Z.; Yao, Z. H.; Wang, J. G. Building highly active hybrid double-atom sites in C_2N for enhanced electrocatalytic hydrogen peroxide synthesis. *Green Energy Environ.* **2021**, *6*, 846–857.
[36] Cheng, T.; Wang, L.; Merinov, B. V.; Goddard, W. A. Explanation of dramatic pH-dependence of hydrogen binding on noble metal electrode: Greatly weakened water adsorption at high pH. *J. Am. Chem. Soc.* **2018**, *140*, 7787–7790.
[37] Zhao, X. H.; Liu, Y. Y. Origin of selective production of hydrogen peroxide by electrochemical oxygen reduction. *J. Am. Chem. Soc.* **2021**, *143*, 9423–9428.
[38] Ramaswamy, N.; Mukerjee, S. Influence of inner- and outer-sphere electron transfer mechanisms during electrocatalysis of oxygen reduction in alkaline media. *J. Phys. Chem. C* **2011**, *115*, 18015–18026.
[39] Ma, B. Y.; Zhao, H. T.; Li, T. S.; Liu, Q.; Luo, Y. S.; Li, C. B.; Lu, S. Y.; Asiri, A. M.; Ma, D. W.; Sun, X. P. Iron-group electrocatalysts for ambient nitrogen reduction reaction in aqueous media. *Nano Res.* **2021**, *14*, 555–569.
[40] Cheng, T.; Fortunelli, A.; Goddard, W. A. Reaction intermediates during operando electrocatalysis identified from full solvent quantum mechanics molecular dynamics. *Proc. Nat. Aca. Sci. USA* **2019**, *116*, 7718–7722.
[41] Su, X.; Yang, X. F.; Huang, Y. Q.; Liu, B.; Zhang, T. Single-atom catalysis toward efficient CO_2 conversion to CO and formate products. *Acc. Chem. Res.* **2019**, *52*, 656–664.
[42] Cui, T. T.; Wang, Y. P.; Ye, T.; Wu, J.; Chen, Z. Q.; Li, J.; Lei, Y. P.; Wang, D. S.; Li, Y. D. Engineering dual single-atom sites on 2D ultrathin N-doped carbon nanosheets attaining ultra-low-temperature zinc-air battery. *Angew. Chem., Int. Ed.* **2022**, *61*, e202115219.
[43] Tang, W. Q.; Yu, H. P.; Cai, C.; Zhao, T.; Lu, C. J.; Zhao, S. L.; Lu, X. H. Solvent effects on a derivative of 1, 3, 4-oxadiazole tautomerization reaction in water: A reaction density functional theory study. *Chem. Eng. Sci.* **2020**, *213*, 115380.
[44] Tang, W. Q.; Zhao, J. H.; Jiang, P.; Xu, X. F.; Zhao, S. L.; Tong, Z. F. Solvent effects on the symmetric and asymmetric SN_2 reactions in the acetonitrile solution: A reaction density functional theory study. *J. Phys. Chem. B* **2020**, *124*, 3114–3122.
[45] Adams, J. S.; Chemburkar, A.; Priyadarshini, P.; Ricciardulli, T.; Lu, Y. B.; Maliekkal, V.; Sampath, A.; Winikoff, S.; Karim, A. M.; Neurock, M. et al. Solvent molecules form surface redox mediators *in situ* and cocatalyze O_2 reduction on Pd. *Science* **2021**, *371*, 626–632.
[46] Zhu, J. J.; Xiao, P.; Li, H. L.; Carabineiro, S. A. C. Graphitic carbon nitride: Synthesis, properties, and applications in catalysis. *ACS Appl. Mater. Interfaces* **2014**, *6*, 16449–16465.
[47] Algara-Siller, G.; Severin, N.; Chong, S. Y.; Björkman, T.; Palgrave, R. G.; Laybourn, A.; Antonietti, M.; Khimyak, Y. Z.; Krasheninnikov, A. V.; Rabe, J. P. et al. Triazine-based graphitic carbon nitride: A two-dimensional semiconductor. *Angew. Chem., Int. Ed.* **2014**, *53*, 7450–7455.
[48] Jiao, Y.; Zheng, Y.; Chen, P.; Jaroniec, M.; Qiao, S. Z. Molecular scaffolding strategy with synergistic active centers to facilitate electrocatalytic CO_2 reduction to hydrocarbon/alcohol. *J. Am. Chem. Soc.* **2017**, *139*, 18093–18100.
[49] Kresse, G.; Hafner, J. *Ab initio* molecular dynamics for liquid metals. *Phys. Rev. B* **1993**, *47*, 558–561.
[50] Hongzhiwei Technology, D. S. Version 2021A, China [Online].https://iresearch.net.cn/cloudSoftware.
[51] Blöchl, P. E. Projector augmented-wave method. *Phys. Rev. B* **1994**, *50*, 17953–17979.
[52] Kresse, G.; Furthmüller, J. Efficient iterative schemes for *ab initio* total-energy calculations using a plane-wave basis set. *Phys. Rev. B* **1996**, *55*, 11169–11186.
[53] Ehrlich, S.; Moellmann, J.; Reckien, W.; Bredow, T.; Grimme, S. System-dependent dispersion coefficients for the DFT-D3 treatment of adsorption processes on ionic surfaces. *ChemPhysChem* **2011**, *12*, 3414–3420.
[54] Chen, Z.; Zhao, J. X.; Cabrera, C. R.; Chen, Z. F. Computational screening of efficient single-atom catalysts based on graphitic carbon nitride ($g\text{-}C_3N_4$) for nitrogen electroreduction. *Small Methods* **2019**, *3*, 1800368.